Empirical Constraints on the Cosmic Infrared Background Using Near-Infrared DIRBE Data

Richard G. Arendt[1] and Eli Dwek

NASA's Goddard Space Flight Center

Code 685, Greenbelt, MD, 20771

arendt@stars.gsfc.nasa.gov, edwek@stars.gsfc.nasa.gov

ABSTRACT

Empirical models for emission from stars and the ISM are subtracted from the zodiacal-light-subtracted DIRBE 3.5 μm emission. Because the models are contaminated by unknown levels of the CIB at other near-IR wavelength, the residual is not simply the 3.5 μm Cosmic IR Background, but a linear combination of the background levels at several wavelengths. In spite of this, the residual can be used to place limits on the near-IR CIB intensity if its spectral shape is assumed. Additionally, the residual level is shown to be more nearly isotropic than previous estimates over a much larger fraction of the sky. An excellent correlation of near-IR and far-IR ISM emission provides evidence of the high accuracy of the brighter stellar emission model. The possibility that any residual emission is zodiacal in nature is discussed.

1. Introduction

TBD: The introduction will describe the Cosmic Infrared Background (CIB) and its significance. It will describe prior efforts at its detection, and point out successes and limitations, setting the stage for the new modeling presented here. Hauser et al. (1998), Arendt & Dwek (1998), Gorjian, Wright, & Chary (2000), Matsumoto, et al. (2000), Kashlinsky, et al. (1996a, 1996b), Kashlinsky & Odenwald (2000).

2. The Models

At the far-IR wavelengths Hauser et al. (1998) modeled the ISM emission at 140 and 240 μm by assuming that it was linearly correlated with the 100 μm emission that was used as a template. This worked moderately well at high latitudes, but left obvious defects especially at low latitudes. The reason is that that linear scaling of the 100 μm ISM template by a single constant coefficient assumes that all of the ISM emission has the same spectrum. Thus regions warmer or colder than average show up as positive or negative residuals. An improved model was found by noting that the ISM emission followed a well-defined trend in color-color plots. The narrow trend implied that the 240 μm ISM emission could be modeled as a linear combination of the 100 and 140 μm emission. The differences between the two ISM templates would account

[1]Raytheon ITSS

for variations in the spectrum of the ISM even when each template is scaled by a single coefficient. Indeed, the isotropy of the residual emission after subtraction of the two-component model was improved enough over a wide range of latitudes to justify the claims for detection of an isotropic CIB.

At near-IR wavelengths, the Dwek & Arendt (1998) approach for modeling the Galactic stellar emission was that of a one-component model. The 2.2 μm emission was scaled by a single coefficient in order to model the stellar emission at each of the other near-IR bands. This empirical model proved to be more accurate than the statistical model used by Hauser et al.(1998), both on the small scales where the statistical model could not match the actual placement of individual stars, and on the large scales, where the statistical model did not properly match the Galactic intensity gradient. However, like the one-component ISM model, the Dwek & Arendt model cannot properly subtract the stellar emission in regions where the mean spectrum changes, caused either by extinction or by changes in the intrinsic colors of the stellar populations. Thus, we seek an improved model of the stellar emission by using a two-component model.

Our basic approach is to model the stellar emission at 3.5 μm as a linear combination of the emission at 2.2 and 4.9 μm:

$$I_{star}(3.5) = AI_{star}(2.2) + BI_{star}(4.9). \tag{1}$$

We refer to this model of the 3.5 μm emission as "Model 1". The model appears to work well at high latitudes, but runs into problems when we try to apply it at low latitudes where extinction affects the stellar colors. Thus, to correct for extinction effects, with the intent that the coefficients A and B will then model intrinsic color variations in the sky brightness, we use the more complicated expression ("Model 2"):

$$I_{star}(3.5) = AI_{star}(2.2)e^{-(\tau_{3.5}-\tau_{2.2})} + BI_{star}(4.9)e^{-(\tau_{3.5}-\tau_{4.9})}. \tag{2}$$

The extinction correction factors are estimated using the fact that

$$\frac{I_{star}(1.25)}{I_{star}(2.2)} \propto e^{-(\tau_{1.25}-\tau_{2.2})}. \tag{3}$$

This ratio of the two shortest wavelength bands is used because extinction will be strongest, and ISM emission appears to be negligible in these bands. Thus, the actual model for the stellar emission we apply is given by

$$I_{star}(3.5) = AI_{star}(2.2)\left[\frac{I_{star}(1.25)}{I_{star}(2.2)}\right]^{\alpha} + BI_{star}(4.9)\left[\frac{I_{star}(1.25)}{I_{star}(2.2)}\right]^{\beta} \tag{4}$$

where $\alpha = (\tau_{3.5} - \tau_{2.2})/(\tau_{1.25} - \tau_{2.2})$ and $\beta = (\tau_{3.5} - \tau_{4.9})/(\tau_{1.25} - \tau_{2.2})$. The numerical values of $\alpha = -0.317$ and $\beta = 0.206$ are calculated using the Rieke & Lebofsky (1985) reddening law, which has been shown to be a good representation of the extinction observed by DIRBE (Arendt et al. 1994).

ISM emission is present at 3.5 μm, though very difficult to see without subtraction of the stellar emission. Our model of the ISM emission will be the simple one-component model used by Hauser et al. (1998):

$$I_{ISM}(3.5) = CI_{ISM}(100) \tag{5}$$

where the 100 μm ISM intensity is the observed emission after subtraction of a 20 nW m^{-2} sr^{-1} estimate of the CIB at that wavelength (Hauser et al. 1998).

The final step is to combine these models with a constant term, D (potentially the isotropic CIB), to model the observed 3.5 μm emission as

$$I_{obs}(3.5) = AI_{obs}(2.2) + BI_{obs}(4.9) + CI_{ISM}(100) + D \tag{6}$$

for Model 1, and

$$I_{obs}(3.5) = AI_{obs}(2.2)\left[\frac{I_{obs}(1.25)}{I_{obs}(2.2)}\right]^{\alpha} + BI_{obs}(4.9)\left[\frac{I_{obs}(1.25)}{I_{obs}(2.2)}\right]^{\beta} + CI_{ISM}(100) + D \quad (7)$$

for Model 2. The coefficients A, B, C, and D can now be determined with a simple least-squares fit. In deriving the solution we excluded the same bright stars and low latitude emission that were excluded at 3.5 μm in the Hauser et al. (1998) analysis. For Model 1, we also found it necessary to exclude regions at low Galactic latitude ($|b| < 10°$), in order to prevent the model from attempting to match low latitude color variations at at the expense of a good fit at high latitudes. The derived values of the model coefficients are listed in Table 1. In Figure 1, we show the residual map that results from subtraction of the stellar and ISM components of each model from the 3.5 micron emission. This residuals have a mean level of D (in the unblanked regions), and are depicted on a comparable intensity range as the Hauser et al. (1998) and Dwek & Arendt (1998) residuals that are also shown in Figure 1.

Note that we actually use the observed 1.25, 2.2, and 4.9 μm intensities in these models rather than only the purely stellar components, since the levels of the CIB at these wavelengths are to be determined. The consequences of this are important, and are discussed in the next section.

3. Interpretation of the Residual

Ideally, if we could have used templates of stellar emission that were free of CIB emission at 1.25, 2.2, and 4.9 μm and free of ISM emission at 4.9 μm, then the residual emission should represent the CIB at 3.5 μm. Instead, these unsubtracted backgrounds propagate through the model and affect the level of the residual. For Model 1, the effects can be traced by rewriting Eq. 6, explicitly identifying all of the components.

$$\begin{aligned} D \;=\; & [I_{star}(3.5) + I_{ISM}(3.5) + I_{CIB}(3.5)] - \\ & A[I_{star}(1.25) + I_{ISM}(1.25) + I_{CIB}(1.25)] - \\ & B[I_{star}(3.5) + I_{ISM}(3.5) + I_{CIB}(3.5)] - \\ & CI_{ISM}(100) \end{aligned} \quad (8)$$

Next, if we assume that the stellar and ISM models are good {i.e. $I_{star}(3.5) = AI_{star}(2.2) + BI_{star}(4.9)$ and $I_{ISM}(3.5) = BI_{ISM}(4.9) + CI_{ISM}(100)$}, then the constant term D can be expressed as a function of the CIB intensity at several wavelengths:

$$D = I_{CIB}(3.5) - AI_{CIB}(2.2) - BI_{CIB}(4.9). \quad (9)$$

When we apply the coefficients derived for Model 1, this expression becomes:

$$D = I_{CIB}(3.5) - 0.445I_{CIB}(2.2) - 0.220I_{CIB}(4.9) = -0.00106 \quad (10)$$

where all intensities are in MJy sr^{-1}, or

$$D = \nu I_{CIB}(3.5) - 0.279\ \nu I_{CIB}(2.2) - 0.308\ \nu I_{CIB}(4.9) = -0.91 \quad (11)$$

with the νI_{ν} in nW m^{-2} sr^{-1}.

For Model 2, the extinction correction makes the equivalent expressions more complex, but with some algebraic reshuffling and keeping only first-order terms, we find

$$\begin{aligned} D \;=\; & I_{CIB}(3.5) - [A\alpha r_{12}^{\alpha-1} + B\beta r_{12}^{\beta} r_{41}]I_{CIB}(1.25) - \\ & [A(1-\alpha)r_{12}^{\alpha} + B\beta r_{12}^{\beta} r_{42}]I_{CIB}(2.2) - Br_{12}^{\beta} I_{CIB}(4.9) \end{aligned} \quad (12)$$

where $r_{12} = I_{star}(1.25)/I_{star}(2.2)$, etc. Inserting the numerical values for $r_{12} = 1.2$, $r_{41} = 0.25$, $r_{42} = 0.3$ and for the other terms, we finally arrive at

$$D = I_{CIB}(3.5) + 0.103 I_{CIB}(1.25) - 0.564 I_{CIB}(2.2) - 0.259 I_{CIB}(4.9) = -0.00234 \quad (13)$$

where all intensities are in MJy sr $^{-1}$, or

$$D = \nu I_{CIB}(3.5) + 0.0386\ \nu I_{CIB}(1.25) - 0.355\ \nu I_{CIB}(2.2) - 0.363\ \nu I_{CIB}(4.9) = -2.01 \quad (14)$$

with the νI_ν in nW m^{-2} sr $^{-1}$.

The above expressions show that for both Model 1 or Model 2, the unsubtracted backgrounds in the 2.2 and 4.9 μm components of the models reduce the value of the residual D from the level of the 3.5 μm CIB. Conversely, the 1.25 μm component adds a small amount to the residual level in Model 2. If the 100 μm CIB had not been subtracted from the template of the ISM emission it would also reduce the observed residual levels by $-0.0387\ \nu I_{CIB}(100)$ nW m^{-2} sr^{-1} in Model 1, or $-0.0347\ \nu I_{CIB}(100)$ nW m^{-2} sr^{-1} in Model 2.

As discussed by Hauser et al. (1998), the systematic uncertainties dominate the random statistical uncertainties in obtaining the mean 3.5 μm residual. Systematic uncertainties include the detector offset and zodiacal light uncertainties, and the uncertainty in the stellar and ISM model developed here. The zodiacal light uncertainties used by Hauser et al. (1998) are equally appropriate here, and are reproduced in Table 2. Detector offset uncertainties are negligible in comparison, and are therefore not listed. The 1 σ uncertainties in the new stellar and ISM models are estimated by using the full variation in the mean residual intensity of the various high latitude regions listed in Table 3 (see below). As in Hauser et al. (1998), we take the quadrature sum of the zodiacal light and combined stellar and ISM uncertainties to arrive at the total systematic uncertainties, listed for each model in Table 2. The scale factors that are applied to the zodiacal light uncertainties are the same as those used to scale each wavelength in the construction of the stellar and ISM models.

4. Isotropy of the Residual

While the residual emission derived here after subtraction of the 3.5 μm stellar and ISM models is not the CIB directly, it should still be isotropic if the models are accurate. Therefore, following the example of Hauser et al. (1998), we have examined several different means of assessing isotropy. In all cases, the key issue is whether or not the data show only the amount of variation expected within the uncertainties.

4.1. Mean Patch Brightness

The simplest test of isotropy is comparison of the mean brightness in selected patches. Table 3 lists the brightnesses derived at several of the regions examined by Hauser et al. (1998) and Dwek & Arendt (1998). The present variation in brightness among these patches is smaller than in either of the two previous studies, and is smaller than the expected systematic uncertainty (even if only the zodiacal light component of the uncertainty is considered). The patch intensities for Model 1 are not quite as uniform as those for Model 2, but in both cases the variations smaller than the expected systematic uncertainties.

4.2. Brightness Distributions

The next isotropy test is the examination of the intensity histograms of the residual emission. For a truly isotropic residual, the shape and width of the histograms will reflect only the random noise uncertainties. Histograms constructed for the north and south portions of the high-latitude HQA and HQB regions examined by Hauser et al. (1998) are shown in Figures 2 and 3. The results of fitting Gaussian distributions to the histograms are shown in the figures and listed in Table 4. The new results exhibit smaller dispersion than the previous results, particularly over the relatively large HQA regions. North-south asymmetries in the means of the distributions are also reduced in the new results. Kolmogorov-Smirnov (K-S) tests applied to the distributions, indicate that the HQBN residuals are essentially Gaussian for the new results with Model 1 and especially Model 2, while distributions in the HQBS (and for the Dwek & and Arendt (1998) HQB regions) are probably only slightly non-Gaussian. The K-S probabilities of the distributions differing from Gaussian are listed in Table 4. A probability of 1.00 is definitely non-Gaussian; a probability of 0.0 indicates a perfectly Gaussian distribution.

4.3. Systematic Spatial Variations

The tests above are necessary conditions for isotropy, but they are insensitive to any anisotropic structure that does not alter the mean level or introduce some skewness or tails to the brightness distributions. A simple means of looking for likely spatial structure is to check for gradients in the residual emission. Figure 4 shows the gradients in the residual emission as a function of the cosecant of Galactic latitude. Data for the north and south hemispheres are shown separately. By this test, the Dwek & Arendt (1998) model removed Galactic emission more effectively than the models used by Hauser et al. (1998). The present models are seen to make further improvements, most dramatically at lower latitudes. The residual emission of Model 2 exhibits smaller gradients than that of Model 1 over this range of latitudes. Table 5 lists the gradients for the HQA and HQB regions, showing no significant Galactic gradient in the HQB region for the residual emission derived from Model 2. The derived gradients in the HQA region are even smaller, but statistically significant as the region is about ten times larger.

4.4. Two-Point Correlation Functions

The most rigorous test of spatial isotropy that was used by Hauser et al. (1998) is the two-point correlation function. A truly isotropic residual should show no structure above the expected random noise on any spatial scales. The two-point correlation functions for the 3.5 μm residual emission from the present and previous results are shown in Figure 5. Note that because the Hauser et al. (1998) results relied on a statistical model for the stellar emission, the mean level but not the detailed structure of the faint stars was removed from the data. Thus, the Hauser et al. results have a much higher "random" noise level than either the Dwek et al. (1998) or the present results. The variance of the residual emission in the present results is slightly smaller than for the Dwek & Arendt results. The two-point correlation function over the HQB region for Model 1 appears to be very nearly random by this test. The Model 2 results are not quite as isotropic as the Model 1 results, but a distinctly better than the Dwek & Arendt results. Detailed examination of the images (Figure 1) suggests that the 2 point correlation functions in the HQB regions are sensitive to small systematic errors in the structure of the zodiacal light model. With the two-component models used here, errors at different wavelengths partially cancel one another. This cancellation turns out to be slightly more

effective for the parameters of Model 1 than those of Model 2.

5. The Interstellar Medium

A good model of the Galactic stellar emission is necessary tool in the study of the relatively faint Galactic ISM at 3.5 and 4.9 μm. Freudenreich (1996) shows that emission of the ISM can be be traced to high latitudes using the 3.5/2.2 μm colors. Arendt et al. (1998) correlated the variations in the reddening-free near-IR colors with 100 μm ISM emission to derive the 3.5/100 μm and the 4.9/100 μm colors of the ISM. However, the derivation of these colors was restricted to very low galactic latitudes. Now, with the stellar emission models developed here, we can subtract the stellar emission directly, producing a map of the 3.5 μm ISM emission instead of only a near-IR color. The 3.5 μm ISM emission derived from subtracting the stellar emission of Model 2 is shown in Figure 6. Comparison with the 100 *micron* emission reveals an excellent match of features down to the noise level of the 3.5 μm map. The linear correlation of the 100 and 3.5 μm emission is plotted in Figure 7 for regions $|b| < 20°$. The linear trend plotted is that derived from Model 2. The inset of shows that the linear trend fits all the way down to the faintest ISM emission. High latitude emission is all faint, and adds noise to the correlation at low intensities, but it still appears to follow the same correlation.

6. Discussion

TBD: The discussion will show how the constraints imposed by the new models can be used to estimate the 4.9 μm CIB based on prior estimates of the 2.2 and 3.5 μm CIB. Figure 8 shows how all bands are constrained by various models and measurements, assuming a blackbody CIB function as an example. A more complicated CIB spectrum may be similarly depicted. Cautionary statements will be made about the similarity of the apparent CIB spectrum to the stellar and *particularly* the zodiacal light spectrum.

7. Summary

TBD: A summary, similar to the abstract, will appear here. Emphasis on the necessity for definite improvements in the zodiacal light modeling as the remaining major step in improving the detection of the near-IR CIB.

This work was supported by the NASA ADP program, grant NASW-99228.

REFERENCES

Arendt, R. G., et al, 1994, ApJ, 425, L85

Arendt, R. G., et al. 1998, ApJ, 508, 74

Dwek, E. & Arendt, R. G. 1998, ApJ, 508, L9

Hauser, M. G., et al. 1998, ApJ, 508, 25

Kelsall, T., et al. 1998, ApJ, 508, 44

Rieke, G. H. & Lebofsky, M. J. 1985, ApJ, 288, 618

...

This preprint was prepared with the AAS LaTeX macros v5.0.

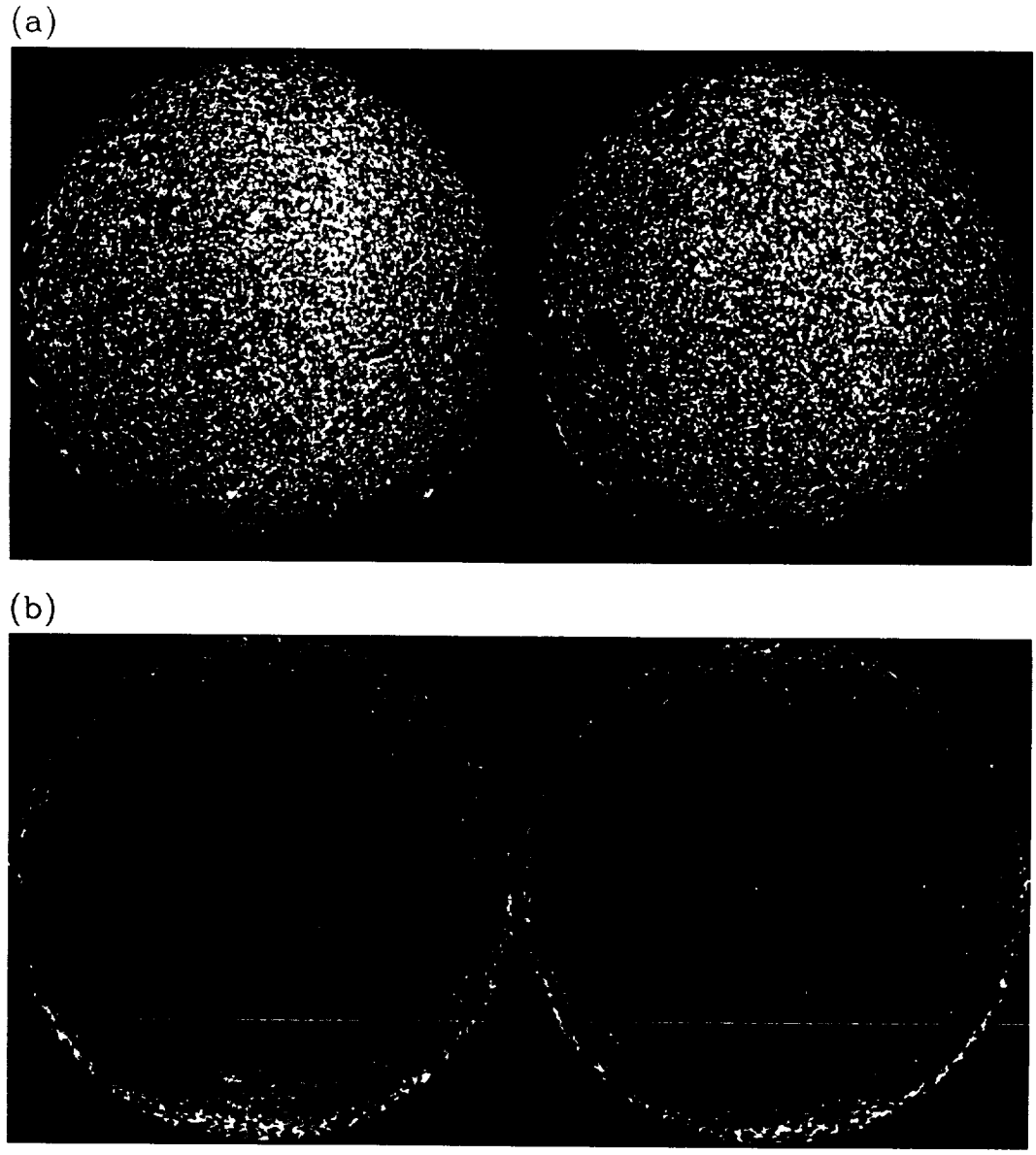

Fig. 1.— Images of 3.5 μm residual emission after subtraction of foreground emission models. (a) Hauser et al. (1998), (b) Dwek & Arendt (1998), (c) Model 1, (d) Model 2. The images are shown as the Galactic azimuthal equal-area projections used by Hauser et al. with the north Galactic hemisphere on the left and south on the right. The Galactic center is at the bottom edge of each hemispherical image. The intensity ranges are linear from -0.01 to 0.05 MJy sr^{-1} for (a) and (b), and -0.0256 to 0.0344 MJy sr^{-1} for (c). The bright source blanking that was applied to the Hauser et al. data was also applied to the other two images.

(c)

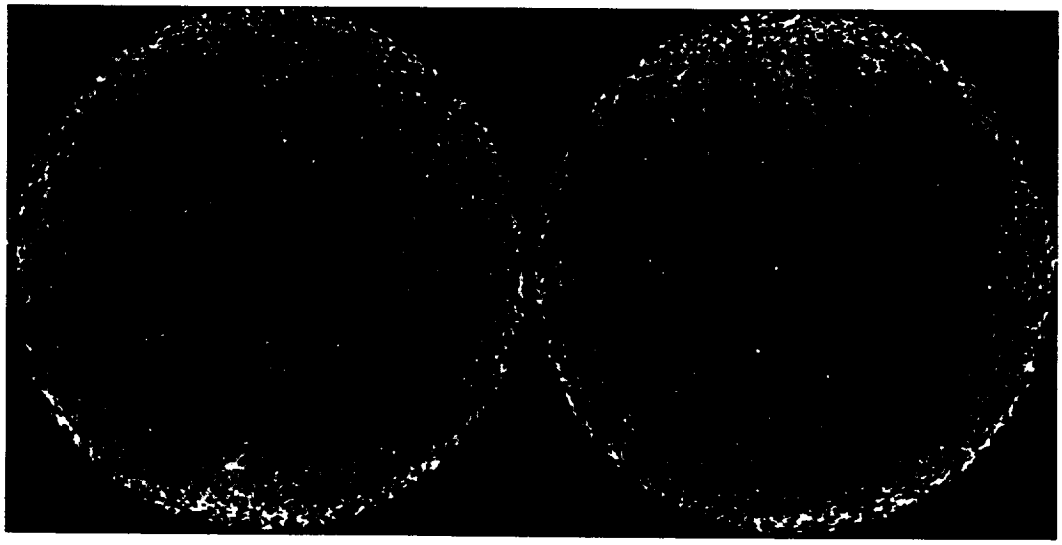

(d)

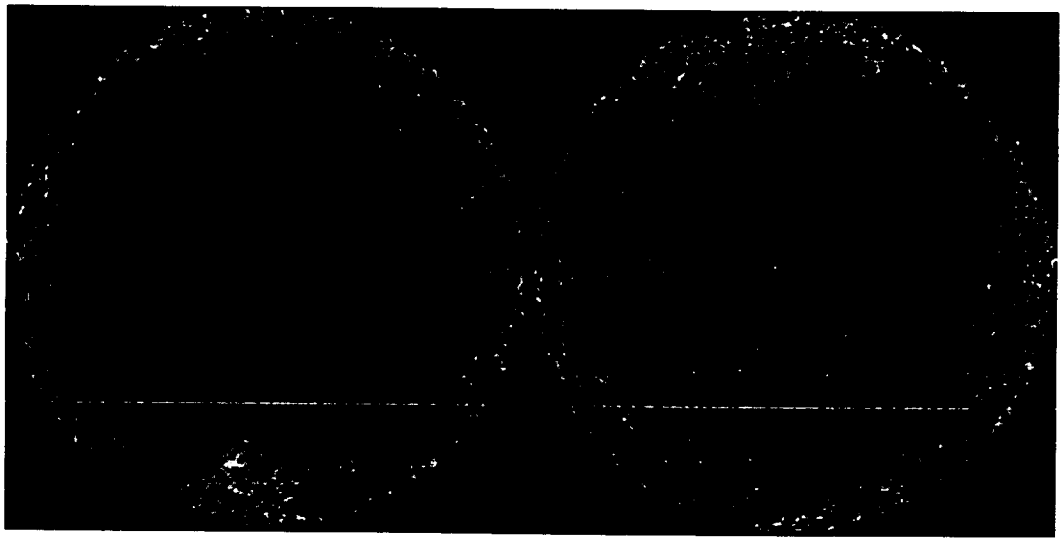

Fig. 1.— *Continued.*

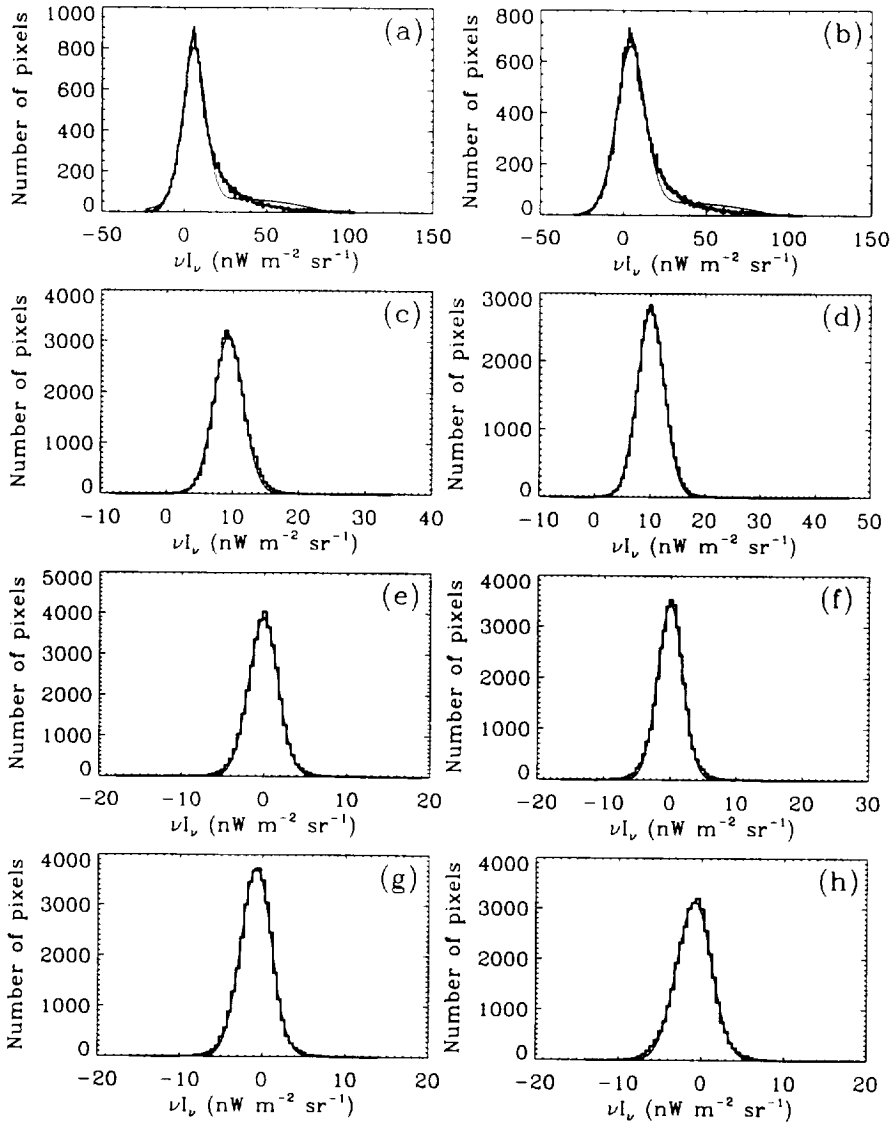

Fig. 2.– Histograms of the residual 3.5 μm intensities in HQAN and HQAS regions from (a,b) the Hauser et al. (1998) results, (c,d) the Dwek & Arendt (1998) results,(e,f) Model 1, and (g, h) Model 2. The smooth lines in panels (c) – (h) show Gaussian fits to the histograms. The histograms in (a) and (b) are fit with an additional parabolic base level, which mitigates the effect of the positive tail on the Gaussian fit to the peak. The HQAN results are on the left, and HQAS results are on the right.

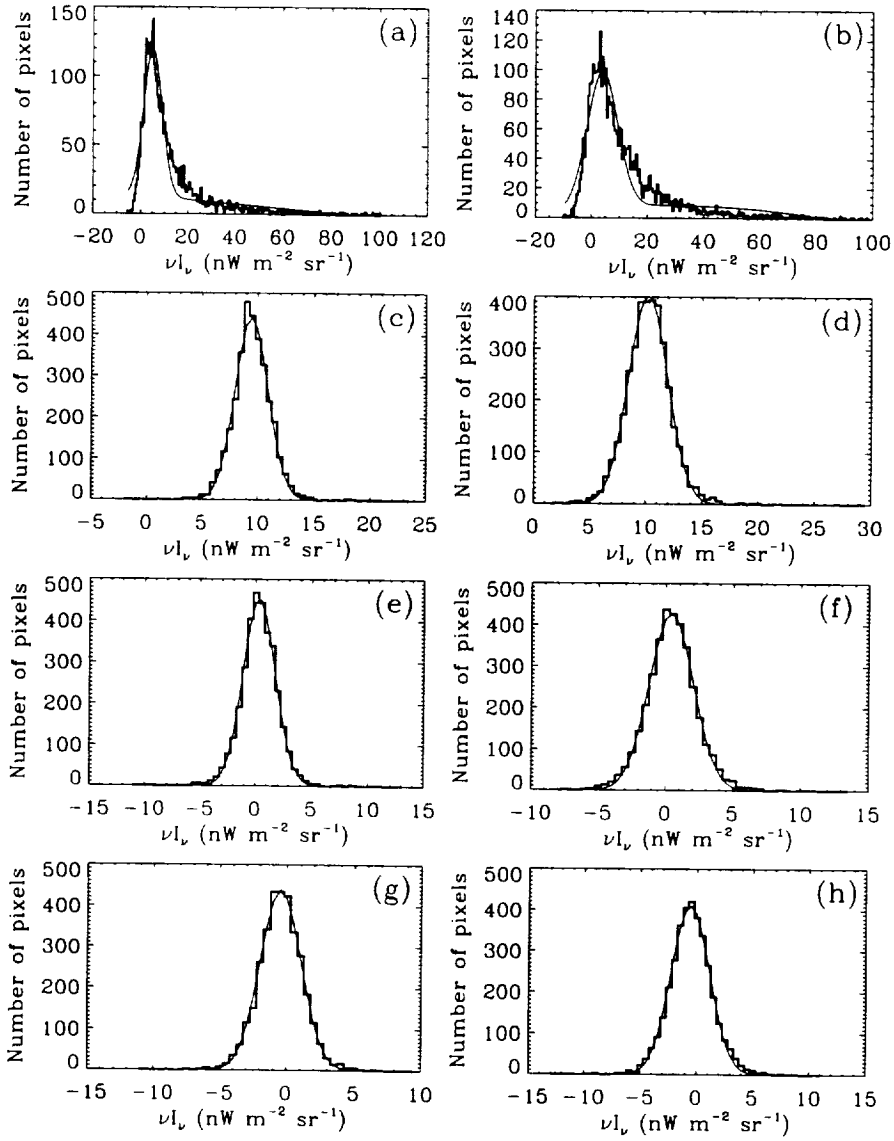

Fig. 3.— Same as Figure 2, but for the smaller HQBN and HQBS regions.

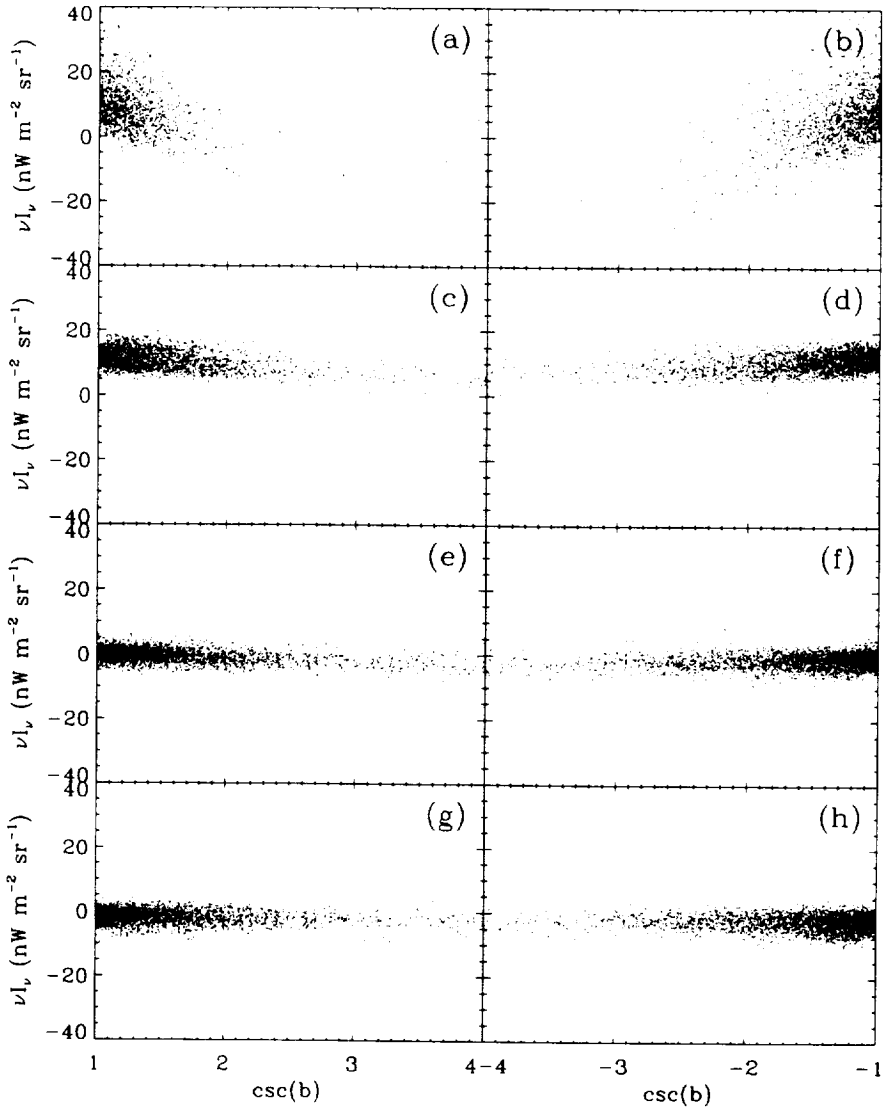

Fig. 4.— Gradients of the residual 3.5 μm emission with respect to the cosecant of the Galactic latitude, $\csc b$. Panels (a,b) show the Hauser et al. (1998) results, (c,d) show the Dwek et al. (1998) results, (e,f) and (g,h) show the results of Model 1 and Model 2. ($\csc 15° \approx 4$, $\csc 30° = 2.0$, and $\csc 60° = 1.15$).

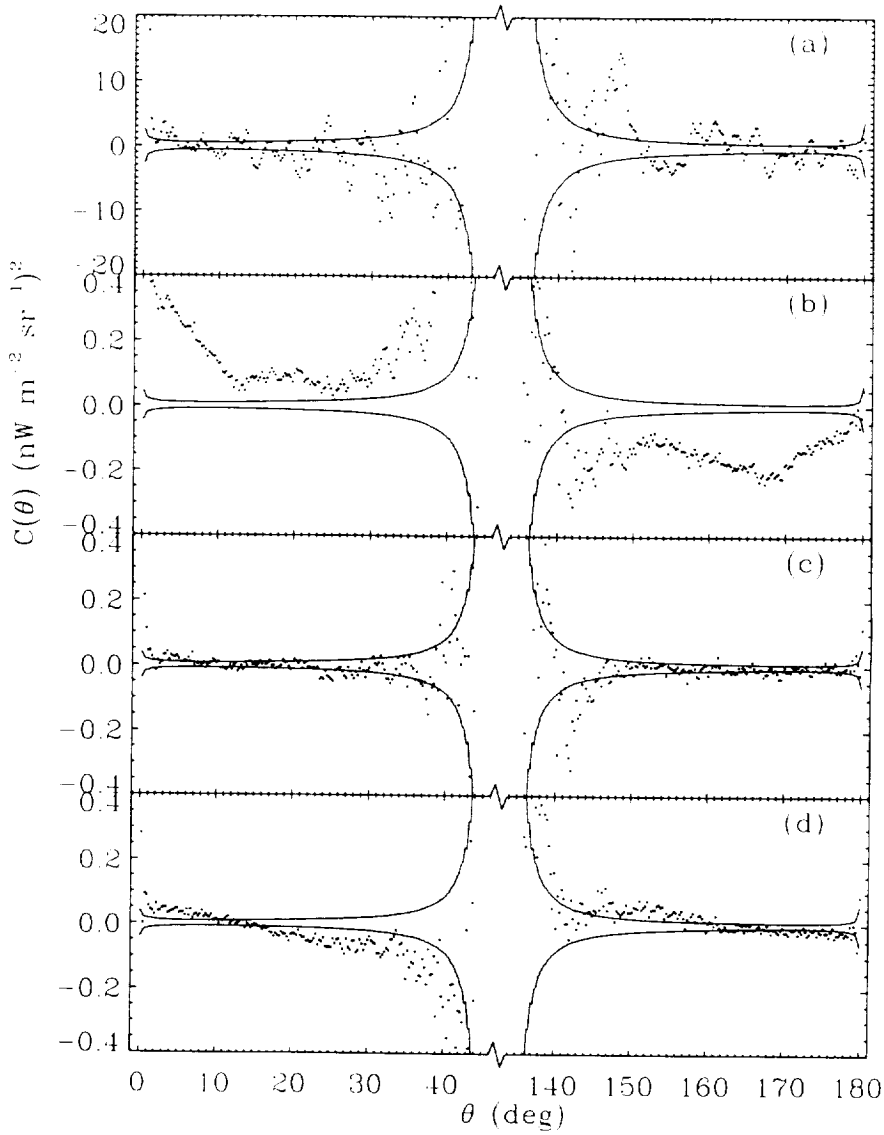

Fig. 5.— Two-point correlation functions of the 3.5 μm residual emission calculated in the HQB regions for (a) the Hauser et al. (1998) result, (b) the Dwek & Arendt (1998) result, (c) the Model 1 result, and (d) the Model 2 result. The solid lines in each panel are the estimated $\pm 1\sigma$ uncertainties.

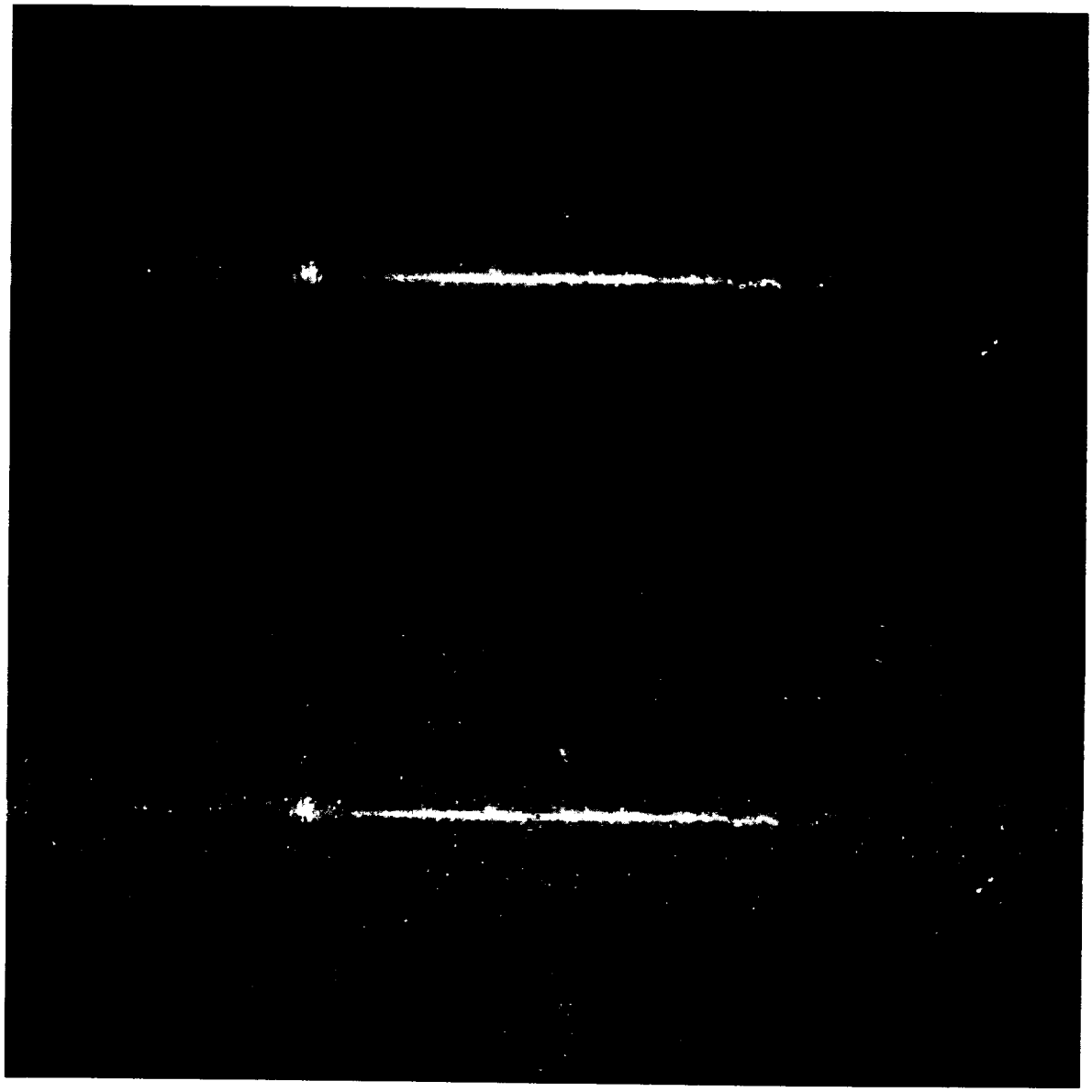

Fig. 6.— The top panel shows the 100 μm ISM emission on a logarithmic intensity scale and a Mollweide projection. The lower panel shows the 3.5 μm ISM emission on a corresponding logarithmic scale, after subtraction of the Model 2 stellar emission. No bright source blanking has been applied.

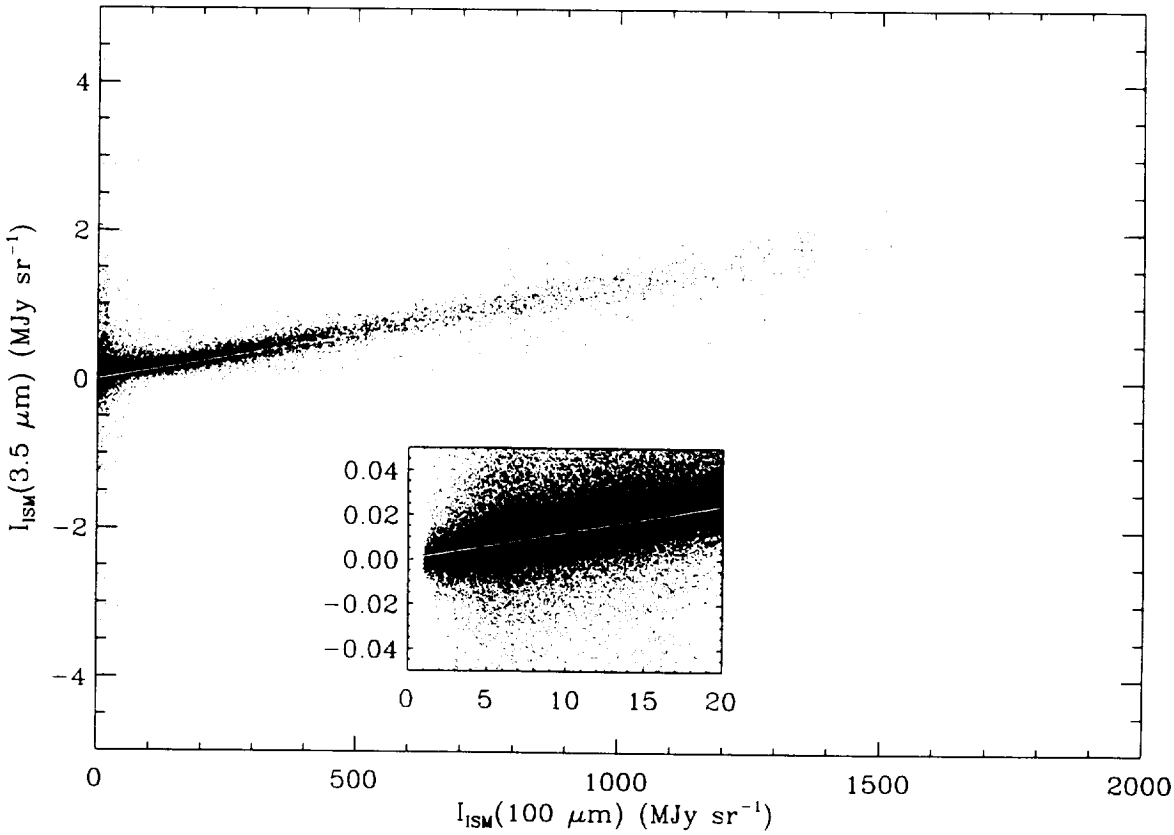

Fig. 7.— ISM emission at 100 and 3.5 μm exhibits a tight linear correlation across a wide range of intensities. The intensities plotted here are from pixels at $|b| < 20°$; higher latitude pixels add more data at the low intensity end of the plot, but do not alter the trend shown in the inset. The slope of the line drawn in the main panel and inset is the parameter C from Model 2 (Table 1).

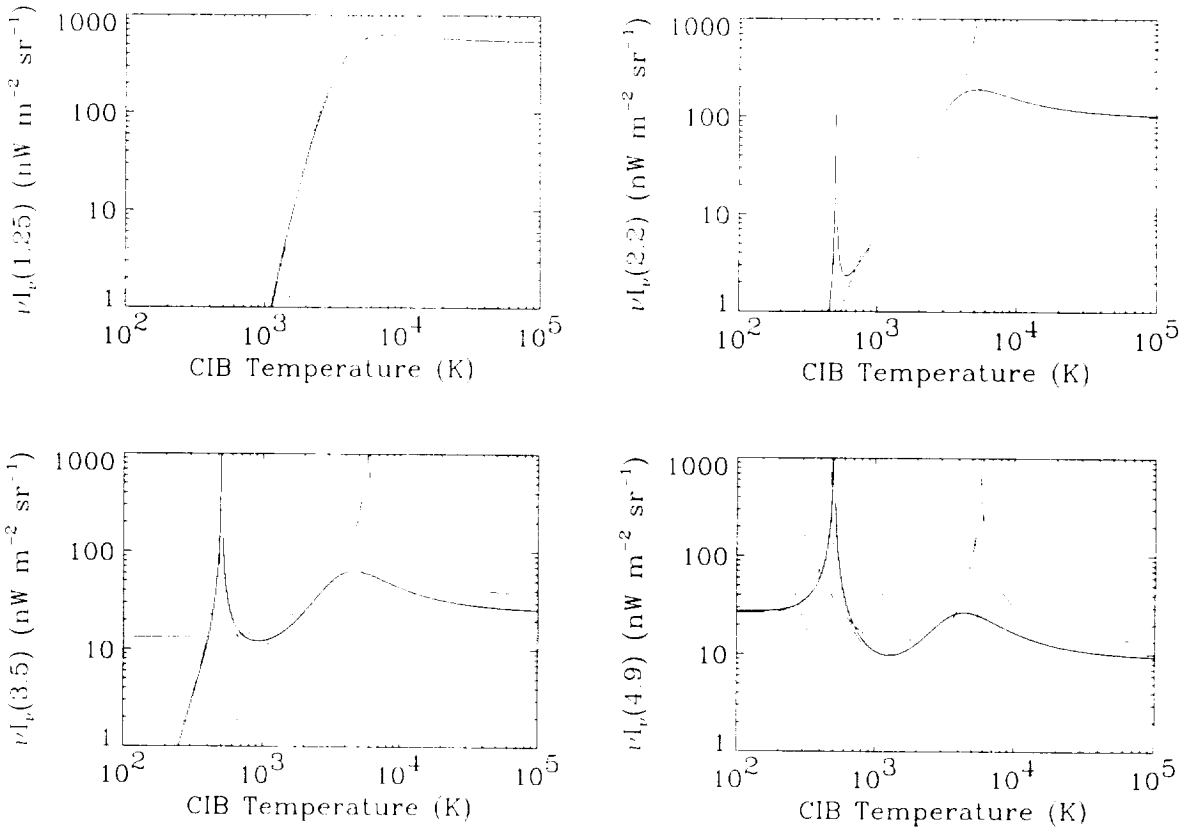

Fig. 8.— Assuming a blackbody spectrum for the CIB, these panels show the various 2 σ upper limits on the intensity at each wavelength, as a function of the CIB temperature. Upper limits from Hauser et al. (1998) are shown as dashed lines. Upper limits imposed by the constraints of Model 1 and Model 2 are shown by the black dashed and solid lines respectively. The Dwek & Arendt (1998) results imply both upper and lower limits on the CIB, which are shown as solid grey lines.

Table 1. Parameters of the 3.5 μm Model

Model Version	A	B	C	D
Dwek & Arendt	0.496	...	0.00183	...
Model 1	0.445	0.220	0.00135	−0.00106
Model 2	0.467	0.250	0.00122	−0.00234

Note. — Values are for I_ν in units of MJy sr^{-1}.

Table 2. Systematic Uncertainties of the Mean 3.5 μm Residual Emission

Uncertainty	Model 1		Model 2	
	σ (nW m^{-2} sr^{-1})	Scale Factor	σ (nW m^{-2} sr^{-1})	Scale Factor
Zodiacal Light (1.25 μm)	...	...	15	0.0368
Zodiacal Light (2.2 μm)	6	0.279	6	0.355
Zodiacal Light (3.5 μm)	2	1.00	2	1.00
Zodiacal Light (4.9 μm)	6	0.308	6	0.363
Zodiacal Light (100 μm)	6	0.0387	6	0.0347
Stellar & ISM Model	2.2	1.00	1.8	1.00
Total	3.9	...	4.1	...

Table 3. Mean 3.5 μm Residual Emission at Select Patches

Patch	Size/Location	Hauser et al. (1998)	Dwek & Arendt (1998)	Model 1	Model 2
NEP	$10° \times 10°$ at $\beta = +90$	5.6	5.8	−1.5	−1.1
SEP	$10° \times 10°$ at $\beta = -90$	−2.3	6.6	−1.0	−0.8
NGP	$10° \times 10°$ at $b = +90$	15.2	11.4	−0.1	−1.6
SGP	$10° \times 10°$ at $b = -90$	15.9	12.7	−0.3	−2.1
LH	$5° \times 5°$ at $(l, b) = (150°, +53°)$	16.1	11.0	0.7	−0.3
HQA	$\|b\| > 30$ and $\|\beta\| > 25$	10.5	9.9	−0.1	−0.9
HQAN	$b > +30$ and $\beta > +25$	11.3	9.5	−0.1	−0.8
HQAS	$\|b\| < -30$ and $\beta < -25$	9.7	10.2	−0.0	−0.9
HQB	$\|b\| > 60$ and $\|\beta\| > 45$	11.4	9.9	0.4	−0.5
HQBN	$b > +60$ and $\beta > +45$	11.7	9.5	0.3	−0.5
HQBS	$b < -60$ and $\beta < -45$	11.0	10.2	0.4	−0.5

Note. — Results are for νI_ν in units of nW m^{-2} sr^{-1}.

Table 4. Gaussian Fits to 3.5 μm Residual Emission Histograms

Model Version	Region	Mean νI_ν (nW m^{-2} sr^{-1})	$\sigma(\nu I_\nu)$ (nW m^{-2} sr^{-1})	K-S Probability Non-Gaussian
Hauser et al. (1998)	HQAN	5.70	6.89	1.00
Hauser et al. (1998)	HQAS	4.25	8.50	1.00
Dwek & Arendt (1998)	HQAN	9.35	2.23	1.00
Dwek & Arendt (1998)	HQAS	10.09	2.43	1.00
Model 1	HQAN	−0.09	1.77	1.00
Model 1	HQAS	−0.05	1.91	1.00
Model 2	HQAN	−0.78	1.85	1.00
Model 2	HQAS	−0.90	2.11	1.00
Hauser et al. (1998)	HQBN	5.05	3.93	1.00
Hauser et al. (1998)	HQBS	3.96	5.47	1.00
Dwek & Arendt (1998)	HQBN	9.44	1.48	0.93
Dwek & Arendt (1998)	HQBS	10.19	1.74	0.92
Model 1	HQBN	0.31	1.45	0.83
Model 1	HQBS	0.40	1.63	0.98
Model 2	HQBN	−0.47	1.50	0.51
Model 2	HQBS	−0.57	1.71	0.96

Table 5. Galactic Gradients of the 3.5 μm Residual Emission

Model Version	Region	Gradient (nW m^{-2} sr^{-1})/csc($\|b\|$)	Correlation Coefficient
Hauser et al. (1998)	HQA	-9.91 ± 0.23	−0.16
Dwek & Arendt (1998)	HQA	-3.32 ± 0.03	−0.34
Model 1	HQA	-0.96 ± 0.03	−0.12
Model 2	HQA	0.39 ± 0.03	0.05
Hauser et al. (1998)	HQB	-19.45 ± 5.32	−0.04
Dwek & Arendt (1998)	HQB	-8.61 ± 0.70	−0.14
Model 1	HQB	-2.53 ± 0.66	−0.05
Model 2	HQB	1.39 ± 0.67	0.02

REPORT DOCUMENTATION PAGE

Form Approved
OMB No. 0704-0188

1. AGENCY USE ONLY *(Leave blank)*

2. REPORT DATE
29 Dec 00

3. REPORT TYPE AND DATES COVERED
Final, 3 Jan 00 - 3 1 Dec 00

4. TITLE AND SUBTITLE
Detection of the Near-IR Cosmic Infrared Background Using Alternative Models of Near-IR Galactic Emission in the DIRBE Data

5.FUNDING NUMBERS
C: NASW-99228
PR/TA: 3458

6.AUTHORS
Richard G. Arendt

7.PERFORMING ORGANIZATION NAME(S) AND ADDRESS(ES)
Raytheon Technical Services Company
Information Technology and Scientific Services
4400 Forbes Boulevard
Lanham, Maryland 20706-4392 USA

8. PERFORMING ORGANIZATION REPORT NUMBER

8.SPONSORING/MONITORING AGENCY NAME(S) AND ADDRESS(ES)
NASA/GSFC
Headquarters Procurement Office
Attn: Kimberly Wiggins/Code 216
Greenbelt, MD 20771

10. SPONSORING/MONITORING AGENCY REPORT NUMBER

11. SUPPLEMENTARY NOTES

12a. DISTRIBUTION/AVAILABILITY STATEMENT

12b. DISTRIBUTION CODE

13. ABSTRACT *(Maximum 200 words)*

The analysis portion of this task has been completed. New models were developed for the removal of the near-infrared emission of Galactic stars in the DIRBE data. Subtraction of these models from the observed emission attempted to achieve a better detection of the Cosmic Infrared Background at near-infrared wavelengths. The new models were found to provide a large improvement in the isotropy of the residual emission, however constraints on the intensity of the emission are not significantly improved. A paper detailing the procedures and results has been drafted, and will be completed next year. The draft of this paper is included as the final report on the contract.

14. SUBJECT TERMS

15. NUMBER OF PAGES
1

16. PRICE CODE

17. SECURITY CLASSIFICATION OF REPORT	18. SECURITY CLASSIFICATION OF THIS PAGE	19. SECURITY CLASSIFICATION OF ABSTRACT	20. LIMITATION OF ABSTRACT
UNCLASSIFIED	UNCLASSIFIED	UNCLASSIFIED	